# Supporting Information

## Synthesis of mechanically stable polybenzoxazine-based porous carbon and their application as high-performance supercapacitor electrodes

Periyasamy Thirukumaran[a,1], Raji Atchudan[a,1], Asrafali Shakila Parveen[b,1], Yong Rok Lee[a], Seong-Cheol Kim[a,*]

[a]School of Chemical Engineering, Yeungnam University, Gyeongsan 38541, Republic of Korea.

[b]School of Material Science and Engineering, Myongji University, Republic of Korea.

[1]Authors contributed equally to this work.

**Synthesized of benzoxazines monomers (AP-f Bzo)**

The multifunctional benzoxazines monomers were synthesized from apigenin and furfuryl amine (AP-f Bzo) through the mannich reaction of triazine according to our previously reported procedure in Ref. 1 with some amendments as shown in Scheme S1. In a 500 mL three-necked round bottom flask equipped with a magnetic stirrer, a thermometer and a reflux condenser, furfurylamine (18.06 g), paraformaldehyde (5.4 g) and DMSO 300 mL were successively added. The reaction system was gently heated up to 100 °C and refluxed under continuous magnetic stirring for 1 h. Then 16.2 g of apigenin and 5.4 g of formaldehyde was added dropwise and the mixture was stirred under a nitrogen atmosphere at 100 °C for 5 h. A homogeneous transparent yellow liquid was obtained. After cooling to room temperature, the reaction mixture was poured into 1 L of 1 N NaOH solution. The precipitate formed was collected by filtration, washed several times with water, and finally washed with ethanol. After drying at 60 °C in a vacuum oven, the dried sample was ground and pale yellow powder of benzoxazine was obtained denoted as AP-f benzoxazine precursor.

**Characterization of the benzoxazine monomer**

The precursor of polybenzoxazine-based nitrogen-rich carbons was synthesized by the Mannich reaction. Novel porous and high surface area carbons were obtained after carbonization and activation. Fourier transform infrared (FTIR) spectrum of the benzoxazine monomer (AP-f) was recorded and is shown in Figure S1. The specific adsorption band at 2846 and at 2962 $cm^{-1}$ were obtained confirming the symmetric and anti-symmetric stretching modes of the $CH_2$ groups in between oxazine ring and furan ring, due to the contribution from the symmetric and anti-symmetric stretching vibration in $CH_2$ of oxazine ring respectively.[1]

There is no brad peak at 3300 $cm^{-1}$ as all –OH groups are completely reacted with the amine group to form oxazine ring. The peak at 1654 $cm^{-1}$ is due to the carbonyl stretching vibration of apigenin moiety. The characteristic absorptions of the oxazine ring structure of AP-f were seen at 1026 and 1226 $cm^{-1}$, attributed to the symmetric and asymmetric stretching modes of C−O−C, respectively, while the peak at 937 $cm^{-1}$ approves the formation of an oxazine ring. Also, the spectrum shows a peak at 1148 $cm^{-1}$ due to the C−N−C symmetric stretching vibrations. The peaks observed at 1584, 989, and 728 $cm^{-1}$ are attributed to the vibrations of the furan ring[2].

The $^{1}$H-NMR spectrum shown in Fig. S2 further confirms the structure of AP-f monomer having three different oxazine rings has resonance peaks at 5.1, 4.8 and 4.7 ppm and 3.7, 3.8 and 3.9 ppm that are assigned to Ar−$CH_2$−N and O−$CH_2$−N of the oxazine ring, respectively. The furan ring protons resonate at 6.2 and 7.2 ppm, and the methylene protons (−$CH_2$) connecting the furan and oxazine appeared between 3.4 and 4.4 ppm, respectively. Aromatic protons appear between 7.0 and 7.6 ppm[3,4]. The $^{13}$C-NMR spectrum also confirms the structure of AP-f. The typical carbon resonance of the oxazine ring is found at 82, 87 and 50,

50.2 and 50.4 ppm for Ar− $CH_2$−N and O−$CH_2$−N, respectively. The furan ring carbons of AP-f gave peaks between 100 and 150 ppm. The peak conforming to the −$CH_2$−N of the furan ring appeared at 50 ppm, Other aromatic carbons appear in between 100 and 180 ppm[5,6]. The peak at 40 ppm is due to the solvent peak (DMSO).

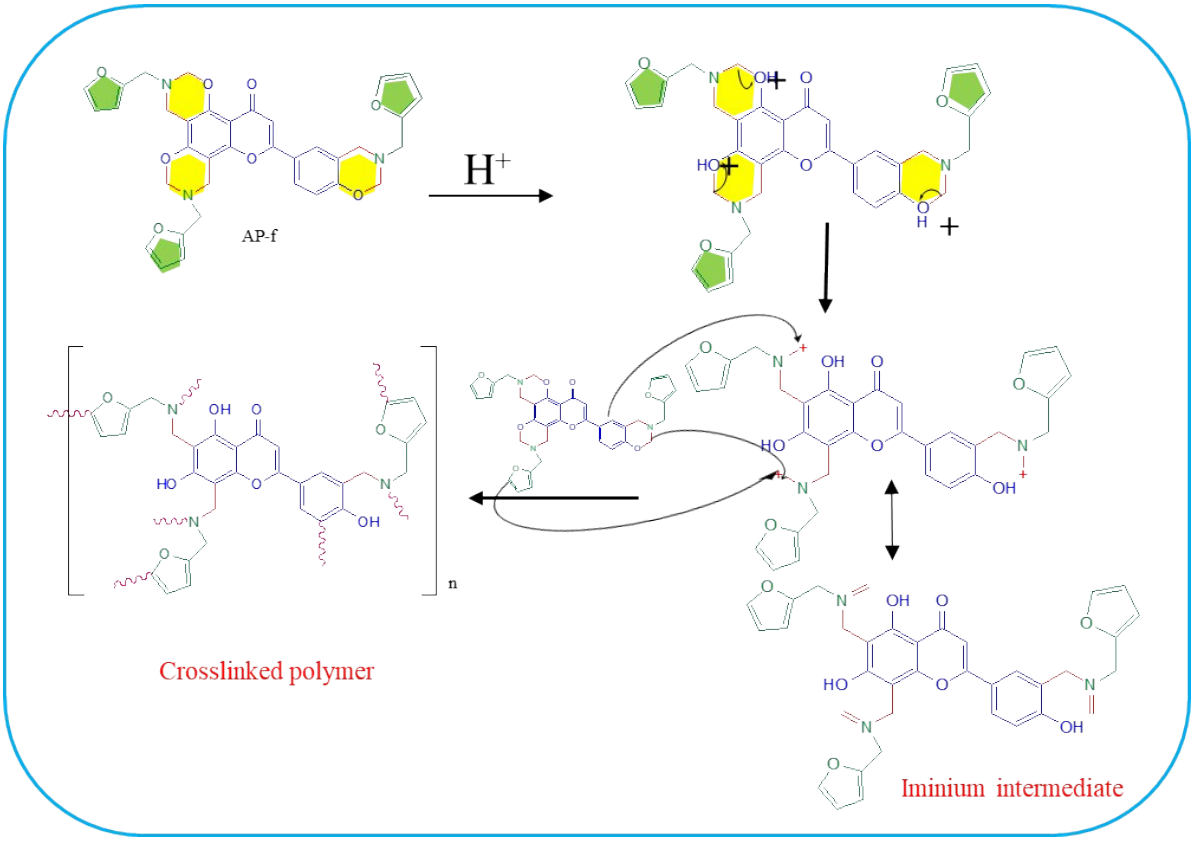


**Scheme S1: Mechanism of acid-catalyzed polymerization of multifunctional benzoxazine monomer**

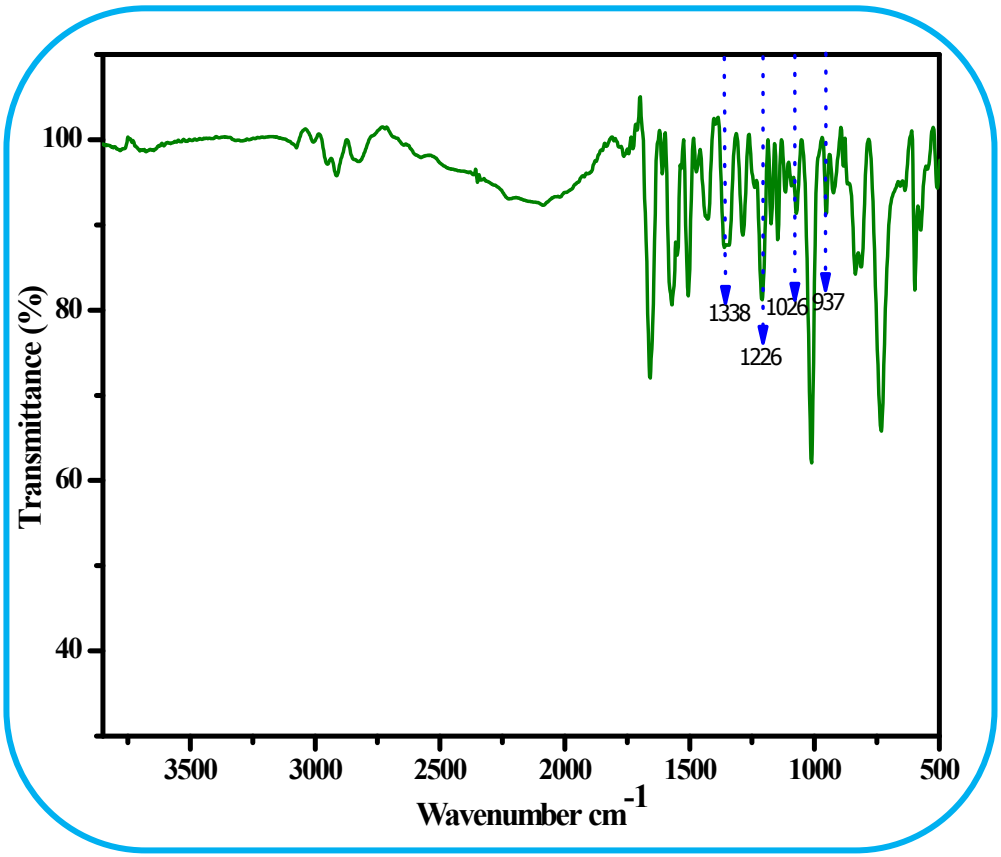


**Figure S1: Fourier transform infrared (FTIR) spectrum of benzoxazine monomer (AP-f)**

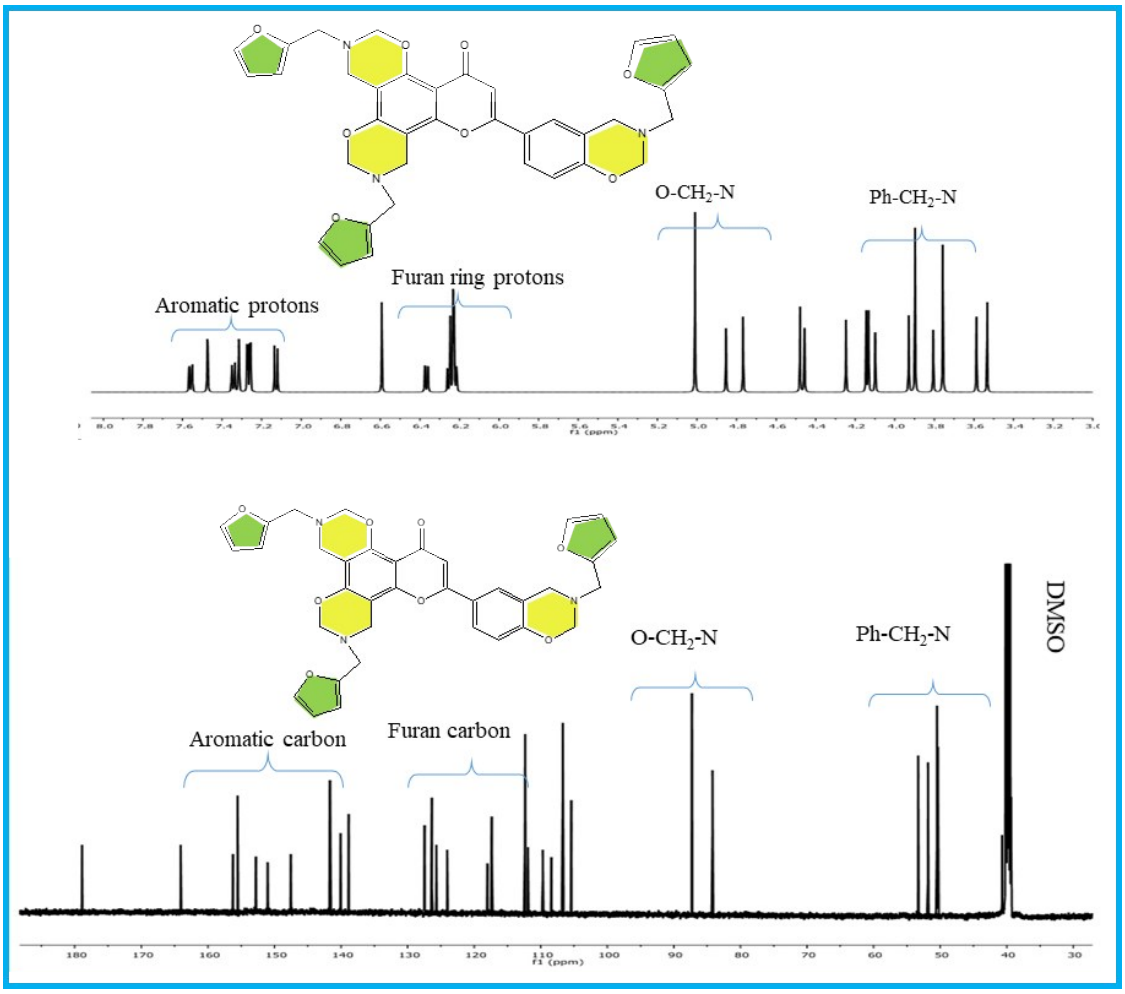


**Figure S2: $^{1}$H-NMR and $^{13}$C-NMR spectrum of benzoxazine monomer (AP-f)**

## Instrumentation methods

The prepared APFC-G and APFC-N materials were characterized by various physicochemical techniques such as field emission scanning electron microscopy (FESEM) with energy-dispersive X-ray spectroscopy (EDS), high-resolution transmittance electron

microscopy (HRTEM), X-ray diffraction (XRD), Raman spectroscopy, nitrogen adsorption-desorption isotherms, attenuated total reflectance Fourier transform infrared (ATR-FTIR) spectroscopy, and X-ray photoelectron spectroscopy (XPS). FESEM with EDS analysis was carried out on a Hitachi S-4800 equipped with EDX at an accelerating voltage of 4 kV. TEM/HRTEM images were performed with an FEI-Tecnai TF-20 transmission electron microscope with an operating accelerating voltage of 120 kV. XRD measurements were carried out using a PANalytical X'Pert$^3$ MRD diffractometer with monochromatized Cu Kα radiation (λ = 1.54 Å) at 40 kV and 30 mA and were recorded in the range from 10 to 90° (2$\theta$). Raman spectrum was recorded on the XploRA Micro-Raman spectrophotometer (Horiba) with the range between 50 and 4000 $cm^{-1}$ at the core research support center for natural products and medical materials of Yeungnam University. Nitrogen sorption isotherms were measured at −197 °C using a Micromeritics ASAP 2000. Before the experiments, the samples were dried at 120 °C and evacuated for 8 h in flowing argon at the flow rate of 60 standard cubic centimeters per minute at 140 °C. Surface area, pore size, and pore volumes were obtained from isotherms using the conventional Brunauer-Emmet-Teller (BET) and Barrett-Joyner-Halenda (BJH) equations. ATR-FTIR spectra were recorded in transmittance mode on a Perkin Elmer Spectrum Two in the wavenumber range from 400 to 4000 $cm^{-1}$ by the addition of 16 scans at a resolution of 16 $cm^{-1}$. XPS spectra were achieved using a K-Alpha (Thermo Scientific). CasaXPS software was used for the deconvolution of the high-resolution XPS spectra.

**Fabrication of working electrode and electrochemical measurements**

The prepared APFC-G and APFC-N materials were used for the fabrication of the working electrode. To fabricate the working electrode, APFC-G or APFC-N materials, and

polyvinylidene fluoride (PVDF) with the wt. % of 95:5 was ground well in an appropriate amount N-Methyl-2-Pyrrolidone (NMP) to make a homogeneous paste, respectively. The resulting homogeneous paste was coated on the conducting substrate (carbon cloth-CC) with an area of 1 $cm^2$ by the drop-casting method and sequentially the electrode was kept at 100 °C in a hot air oven for 48 h to dry the electrodes. After the fabrication, the obtained modified working electrodes were examined for supercapacitor activity. All electrochemical measurements including cyclic voltammetry (CV), galvanostatic charge-discharge (GCD), and electrochemical impedance spectroscopy (EIS) were conducted with a typical three-electrode system and were performed on the CorrTest-CS350 electrochemical workstation in 1 M $H_2SO_4$ aqueous solution. A commercial Ag/AgCl electrode was employed as a reference electrode, a platinum plate (1 $cm^2$) was used as a counter electrode and APFC-G or APFC-N material loaded CC (APFC-G/CC or APFC-N/CC) was used as working electrodes. The CV measurements were carried out at a potential window from 0.0 and 0.7 V (*vs*. Hg/$HgSO_4$) under the different scan rates from 5 to 300 mV $s^{-1}$). The GCD measurements were performed with a potential window of 0.0−0.7 V (*vs*. Hg/$HgSO_4$) at the current densities varied from 0.5 to 10 A $g^{-1}$. EIS measurements were performed in the frequency range of 0.01 kHz–100 kHz with an alternating current amplitude of 5 mV. All the electrochemical tests were conducted at room temperature. The capacitances of the electroactive materials were obtained from their GCD curves according to the following equation (S1)[7].

$$C_s = \frac{I\Delta t}{m\Delta V} \qquad \text{(S1)}$$

whereas, $C_s$ is the specific capacitances (F $g^{-1}$), $I$ is the current in the charge-discharge process (A), $\Delta t$ represents to the discharge time (s), $\Delta V$ stands for the potential window during the charge-discharge measurement (V) and $m$ donates the mass of the electroactive materials (g)

**Two electrode symmetric supercapacitor**

For the two-electrode system, the total mass of active material was maintained to be 60 mg in the assembled cell. The electrochemical performance of two electrode symmetric supercapacitor was evaluated by GCD methods. The specific capacitance of a eletrode ($C_s$), energy density ($E_D$), and power density ($P_D$) of the two-electrode device were calculated using the following Eqs. (S2), (S3) and (S4)[8].

$$C_{gs} = 2\frac{I\Delta t}{m\Delta V} \qquad \text{(S2)}$$

$$E_D = \frac{C_{gs}\Delta V^2}{2\times 3.6} \qquad \text{(S3)}$$

$$P_D = 3600\times\frac{E_D}{\Delta t} \qquad \text{(S4)}$$

where $C_s$ is the specific capacitance, $\Delta V$ is the voltage change of the supercapacitor between completely charged and discharged, and $\Delta t$ is the discharge time.

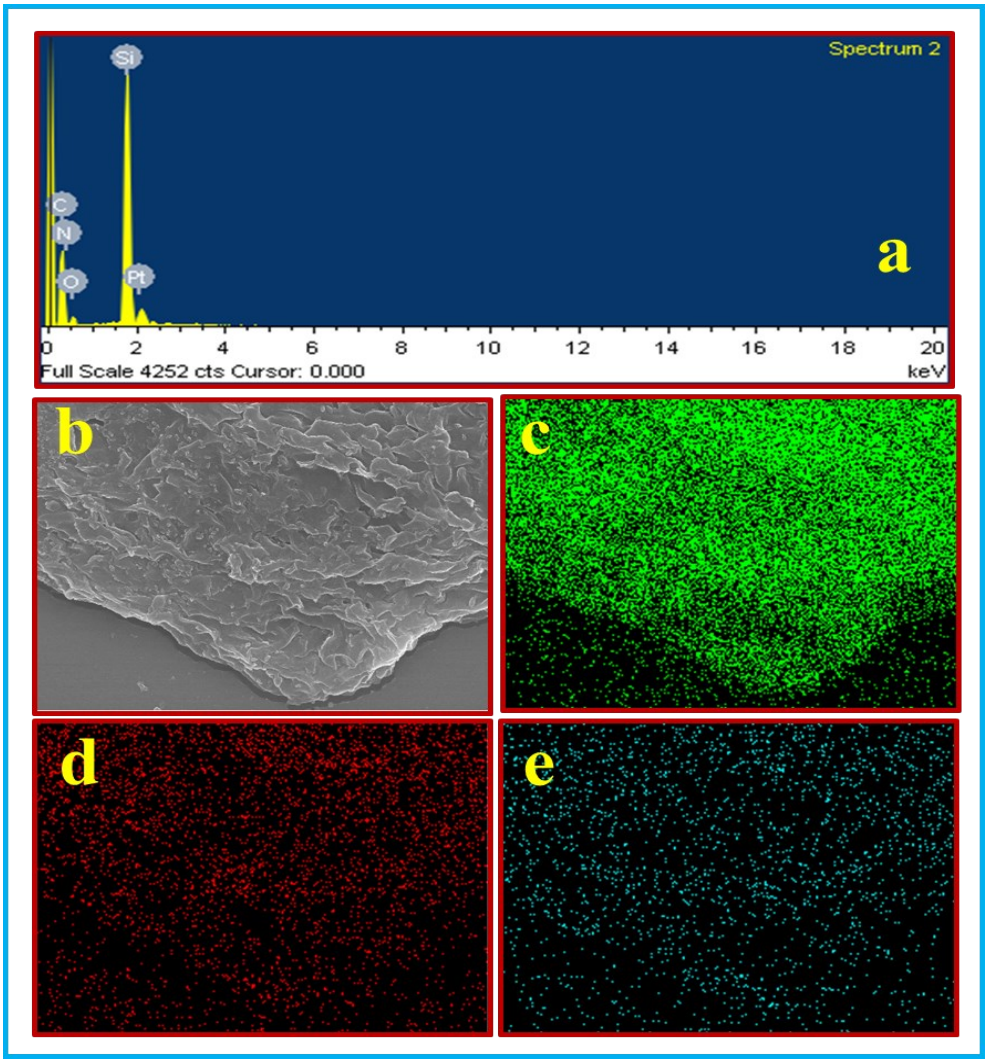


**Figure S3: (a) EDX spectrum of synthesized APFC-N (b) FESEM images and corresponding elemental mapping of (c) carbon (d) oxygen and (e) nitrogen of synthesized APFC-N**

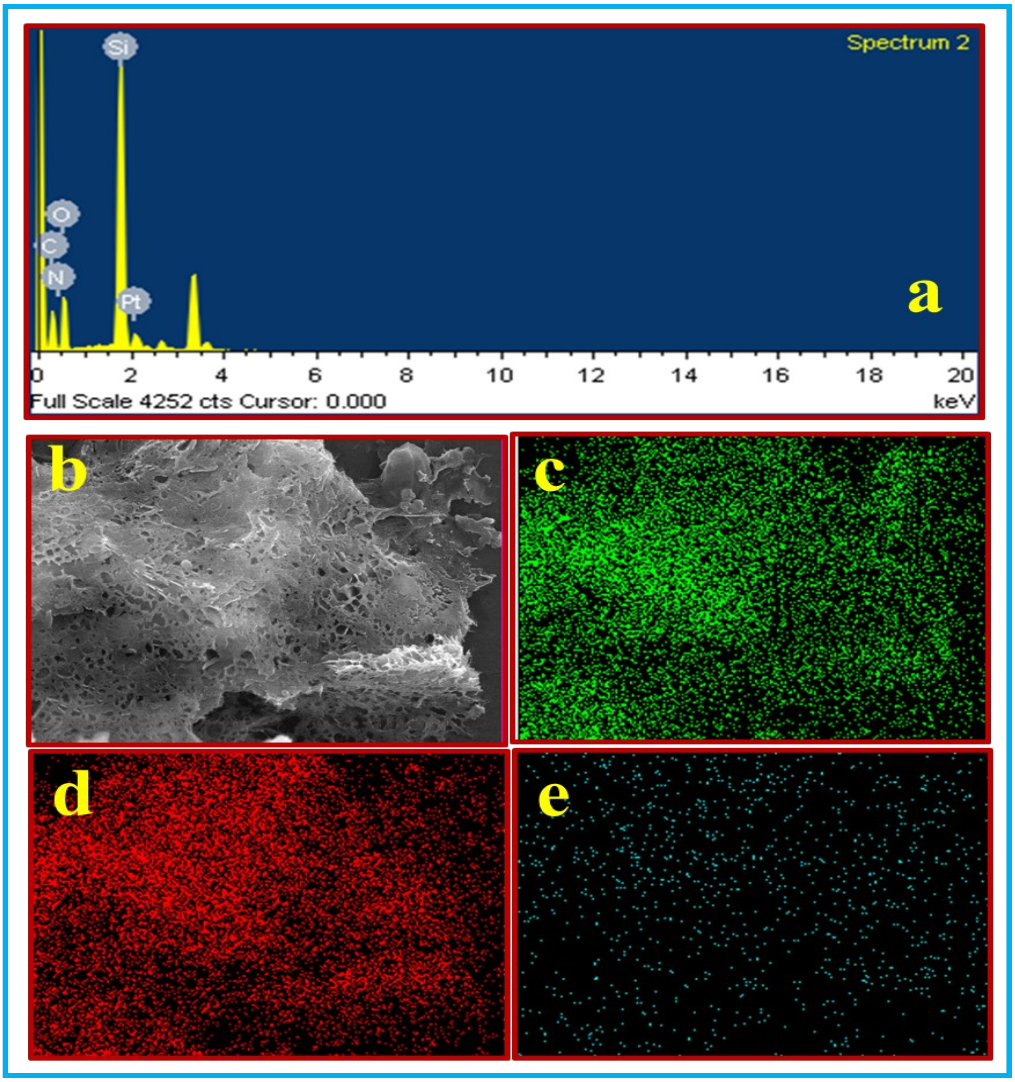


**Figure S4: (a) EDX spectrum of synthesized APFC-G (b) FESEM images and corresponding elemental mapping of (c) carbon (d) oxygen and (e) nitrogen of synthesized APFC-G**

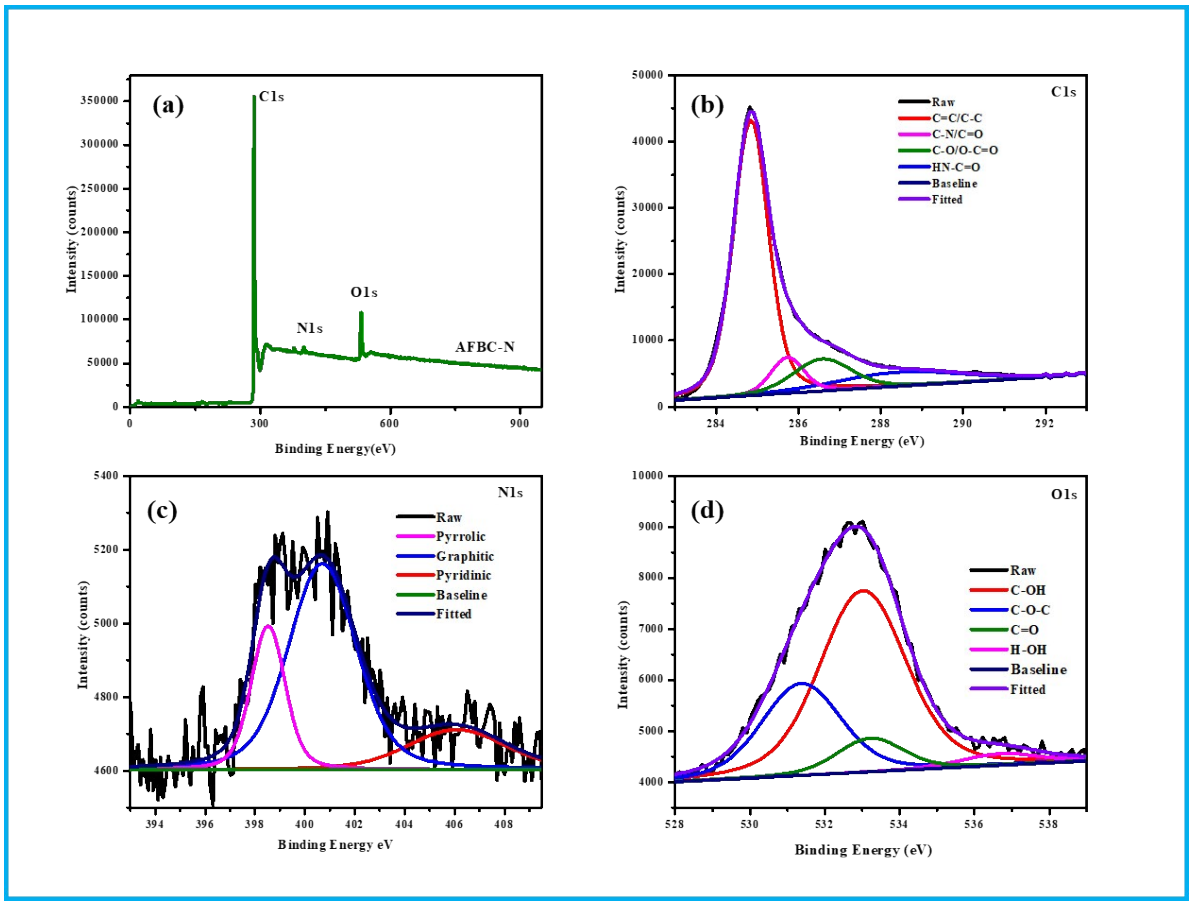


**Figure S5: XPS spectra (a) survey scan (b) C 1s (c) N 1s and (d) O 1s of synthesized APFC-G**

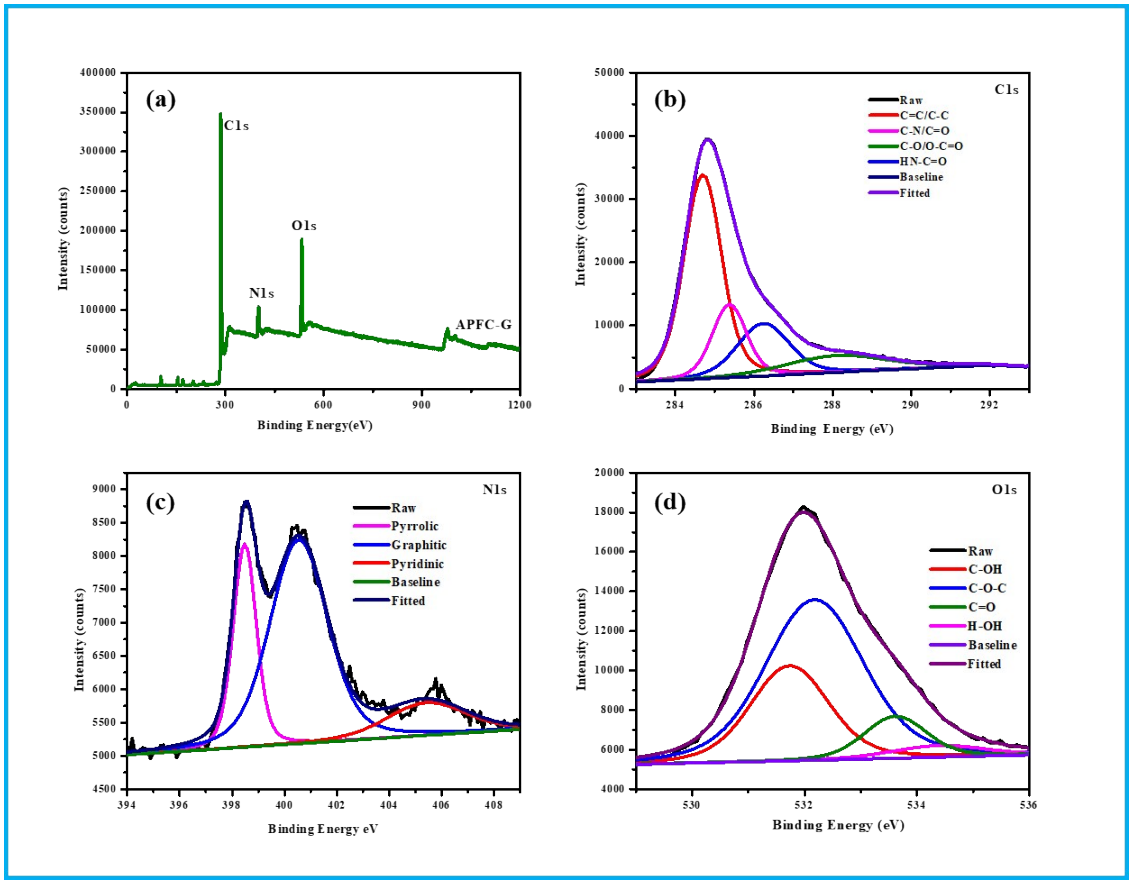


**Figure S6: XPS spectra (a) survey scan (b) C 1s (c) N 1s and (d) O 1s of synthesized APFC-N**

**Table S1: Comparison of specific capacitance of different forms of carbon**

| S. No. | Material | Technique | $C_s$ (F/g) | Measurement condition | Ref. |
|---|---|---|---|---|---|
| 1. | CS | CVD | 132 | 6 M KOH at 1 A/g | 9 |
| 2. | HMCS | CVD | 120 | 1 M $H_2SO_4$ at 1 mV/s | 10 |
| 3. | PCS | Catalytic graphitization | 127 | 2 M KOH at 0.2 A/g | 11 |
| 4. | PCS | Catalytic graphitization | 150 | 6 M KOH at 1 A/g | 12 |
| 5. | MCS | Template method | 146 | 2 M KOH at 1 mV/s | 13 |
| 6. | GNHCS | Carbonization | 120 | 6 M KOH at 0.5 A/g | 14 |
| 7. | NG-900 | Microwave irradiation | 130 | 6 M KOH at 0.5 A/g | 15 |
| 8. | aNG | KOH activation using thermal annealing | 132.4 | 1 M KOH at 0.1 A/g | 16 |
| 9. | BC | Pyrolysis, carbonization and $HNO_3$ activation | 115 | 0.5 mol/$dm^3$ $H_2SO_4$ | 17 |
| 10. | CMG | Functionalization | 135 | 5.5 M KOH at 10 mA | 18 |
| 11. | APFC-G | Gelation, carbonization, KOH activation | 120 | 1 M $H_2SO_4$ at 0.5 A/g | Present work |

$C_s$: specific capacitance; CS: carbon spheres; HMCS: hollow mesoporous carbon spheres; PCS: porous carbon spheres; MCS: mesoporous carbon spheres; GNHCS: graphitic N-doped hollow carbon spheres; NG: nitrogen-doped graphene nanosheets; aNG: activated nitrogen-doped graphene nanosheets; BC: biochar carbon; CMG: chemically modified graphene: APFC-G: Apigenin-furfurylamine based carbon using gelation.

## References


1. A. Trejo-Machin, P. Verge, L. Puchot, R. Quintana, Green Chem. 19 (2017) 5065-5073.
2. C. F. Wang, J. Q. Sun, X. D. Liu, A. Sudo, T. Endo, Green Chem. 14 (2012) 2799-2806.
3. X. Shen, J. Dai, Y. Liu, X. Liu, J. Zhu, Polymer 122 (2017) 258-269.

4. T. Agag, C. R. Arza, F. H. J. Maurer, H. Ishida, Macromolecules 43 (2010) 2748-2758.
5. J. A. Macko, H. Ishida, Polymer 42 (2001) 227-240.
6. T. Takeichi, T. Agag, R. Zeidam, J. Polym. Sci., Part A: Polym. Chem. 39 (2001) 2633-2641.
7. Y. Zou, I. A. Kinloch, R. A. W. Dryfe, ACS Applied Materials & Interfaces 7 (2015) 22831-22838.
8. L. Wan, W. Wei, M. Xie, Y. Zhang, X. Li, R. Xiao, J. Chen, C. Du, Electrochim. Acta 311 (2019) 72-82.
9. J. A. Carrasco, H. Prima-Garcia, J. Romero, J. Hernandez-Saz, S. I. Molina, G. Abellan, E. Corondo, J. Mater. Chem. C 4 (2016) 440-448.
10. X. Chen, K. Kierzek, K. Wenelska, K. Cendrowski, J. Gong, X. Wen, T. Tang, P. K. Chu, E. Mijowska, Chem. -Asian J. 8 (2013) 2627-2633.
11. B. Chang, B. Yang, Y. Guo, Y. Wang, X. Dong, RSC Adv. 5 (2015) 2088-2095.
12. J. Zhu, H. Shi, X. Zhou, Y. Hu, J. Electron. Mater. 46 (2017) 5995-6000.
13. J. Zhou, J. He, C. Zhang, T. Wang, D. Sun, Z. Di, D. Wang, Mater. Character. 61 (2010) 31-38.
14. L. Liu, S. -D. Xu, Q. Yu, F. -Y. Wang, H. -L. Zhu, R. -L. Zhang, X. Liu, Chem. Commun. 52 (2016) 11693-11696.
15. K. H. Lee, J. Oh, J. G. Son, H. Kim, S. S. Lee, ACS Appl. Mater. Interfaces 6 (2014) 6361-6368.
16. B. Zheng, T. -W. Chen, F. -N. Xiao, W. -J. Bao, X. -H. Xia, J. Solid State Electrochem. 17 (2013) 1809-1814.

17. J. Jiang, L. Zhang, X. Wang, N. Holm, K. Rajagopalan, F. Chen, S. Ma, Electrochim. Acta 113 (2013) 481-489.

18. M. D. Stoller, S. Park, Y. Zhu, J. An, R. S. Ruoff, Nano Lett. 8 (2008) 3498-3502.